Geochemistry Geophysics Geosystems G3
AN ELECTRONIC JOURNAL OF THE EARTH SCIENCES
Published by AGU and the Geochemical Society

Article
Volume 4, Number 3
11 March 2003
1026, doi:10.1029/2002GC000415
ISSN: 1525-2027

Observations and models of lateral hydrothermal circulation on a young ridge flank: Numerical evaluation of thermal and chemical constraints

Joshua S. Stein
Department of Earth Sciences, University of California, Santa Cruz, California, USA

Now at Sandia National Laboratories, 4100 National Parks Highway, Carlsbad, New Mexico 88220, USA. (jsstein@sandia.gov)

Andrew T. Fisher
Department of Earth Sciences, University of California, Santa Cruz, California 95064, USA (afisher@es.ucsc.edu)

Center for the Study and Imaging of the Dynamic Earth, University of California, Santa Cruz, California, USA

[1] We used a two-dimensional coupled heat and fluid flow model to investigate large-scale, lateral heat and fluid transport on the eastern flank of the Juan de Fuca Ridge. Cool seawater in the natural system is inferred to enter basement where it is exposed close to the spreading center and flow laterally beneath thick sediments, causing seafloor heat flow to be depressed relative to that input at the base of the plate. The flow rate, and thus the properties of permeable basement (the flow layer), controls the efficiency of lateral heat transport, as quantified through numerical modeling. We simulated forced flow in this layer by pumping water through at a fixed rate and quantified relations between flow rate, thickness of the permeable basement, and the extent of suppression of seafloor heat flow. Free flow simulations, in which fluid flow was not forced, match heat flow constraints if nonhydrostatic initial conditions are used and flow layer permeabilities are set to the high end of observed values (10^{-11} to 10^{-9} m^2). To match seafloor heat flow observations, the models required lateral specific discharge of 1.2 to 40 m/yr for flow layer thicknesses of 600 to 100 m, respectively. The models also replicate differences in fluid pressures in basement, and the local distribution of pressures above and below hydrostatic. Estimated lateral flow rates are 10× to 1000× greater than estimates based on radiocarbon ages of basement pore waters. Estimated lateral flow rates based on thermal and chemical constraints can be reconciled if diffusion from discrete flow zones into less permeable stagnant zones in the crust is considered.

Components: 10,237 words, 11 figures, 1 table.

Keywords: hydrothermal; mid-ocean ridge; heat flow; radiocarbon.

Index Terms: 3015 Marine Geology and Geophysics: Heat flow (benthic) and hydrothermal processes; 3210 Mathematical Geophysics: Modeling; 1832 Hydrology: Groundwater transport.

Received 26 July 2002; **Revised** 16 December 2002; **Accepted** 13 January 2003; **Published** 11 March 2003.

Stein, J. S., and A. T. Fisher, Observations and models of lateral hydrothermal circulation on a young ridge flank: Numerical evaluation of thermal and chemical constraints, *Geochem. Geophys. Geosyst.*, *4*(3), 1026, doi:10.1029/2002GC000415, 2003.

1. Introduction

[2] Hydrothermal circulation through the flanks of mid-ocean ridges (seafloor $\geq$1 m.y. old) accounts for 30% of lithospheric heat loss due to plate cooling [*Stein and Stein*, 1994] and >90% of the global mass flux of water through the oceanic crust [*Mottl and Wheat*, 1994]. This process also influences the physical and chemical state of the crust and overlying ocean [e.g., *Alt*, 1995; *Elderfield and Schultz*, 1996], and supports remarkable biological communities [*Becker et al.*, 2000]. Despite its importance, we know little about the mechanisms by which these systems operate or the spatial and temporal scales of variability. Studying ridge flank circulation is challenging because flanks constitute vast areas of the seafloor, discharge temperatures are much lower than at ridge crests, and fluids generally are not as severely altered. It is occasionally possible to find sites of isolated venting [*Mottl et al.*, 1998], but it is difficult to determine where fluids flowing from these areas originated, how long they spent in the subsurface, and how rapidly they were transported.

[3] Because ridge flanks become covered by sediments as the plate ages, measurements of seafloor heat flow can be used to map out patterns of fluid flow in underlying basement. Deviations of seafloor heat flow from a conductive reference model of the cooling lithosphere [e.g., *Parsons and Sclater*, 1977; *Stein and Stein*, 1994] and the extent to which basement thermal conditions have been homogenized [e.g., *Davis et al.*, 1989; *Fisher et al.*, 1990] may be used to infer the extent and significance of hydrothermal circulation in the crust. As a ridge flank develops a thick and nearly continuous sediment blanket, the rapid exchange of fluid and heat with the overlying ocean becomes focused at widely spaced basement outcrops [*Davis et al.*, 1992; *Thomson et al.*, 1995]. Lateral flow between outcrops can remove much of the heat conducted from the base of the lithosphere before it reaches the seafloor [*Fisher and Becker*, 2000; *Langseth and Herman*, 1981]. Heat flow tends to be most suppressed close to areas of seawater recharge, but lateral flow can occur at geochemically significant rates even after seafloor heat flow observations match conductive models for the cooling plate. Coupled heat and fluid flow models can be applied to lateral flow systems to quantify the conditions under which heat flow anomalies can be explained [e.g., *Davis et al.*, 1997c; *Rosenberg et al.*, 2000; *Wang et al.*, 1997].

[4] Heat flow surveys on several ridge flanks have revealed widespread areas where measured values are lower than expected but rise toward predicted values with increasing distance from the ridge crest. Examples of this phenomenon include the west flank of the Mid-Atlantic Ridge [*Langseth et al.*, 1992; *Langseth and Herman*, 1981; *Langseth et al.*, 1984], the equatorial Pacific [*Baker et al.*, 1991], the south flank of the Costa Rica Rift [*Fisher et al.*, 1990; *Hobart et al.*, 1985; *Langseth et al.*, 1983] and the east flank of the Juan de Fuca Ridge [*Davis et al.*, 1992; *Davis et al.*, 1999]. In some of these areas, pore water chemistry has revealed increasing seawater-basalt reaction along the path of increasing seafloor heat flow [*Baker et al.*, 1991; *Elderfield et al.*, 1999; *Wheat et al.*, 2000], consistent with the idea that fluids may flow laterally over long distances within basement rocks.

[5] In this study, we present results of new finite element models of coupled heat and fluid flow. These models were created to address the following questions: (1) what fluid flow rates and basement properties are required in order to extract heat advectively as indicated by repeated heat flow surveys, (2) are these rates and properties consistent with what is known about oceanic crustal structure and properties and independent estimates made from geochemical observations, and (3) how can discrepancies between estimates based on different methods and assumptions be reconciled? In the next section, we introduce the primary field area and describe estimates of lateral flow rates within the oceanic basement of ridge flanks. We then describe results from a series of numerical simulations intended to address the questions listed above, and discuss what this tells us about the nature of ridge-flank hydrogeology.

2. Field Site: Eastern Flank Juan de Fuca Ridge

[6] The eastern flank of the Endeavour segment of the Juan de Fuca Ridge (Figure 1) is one of the

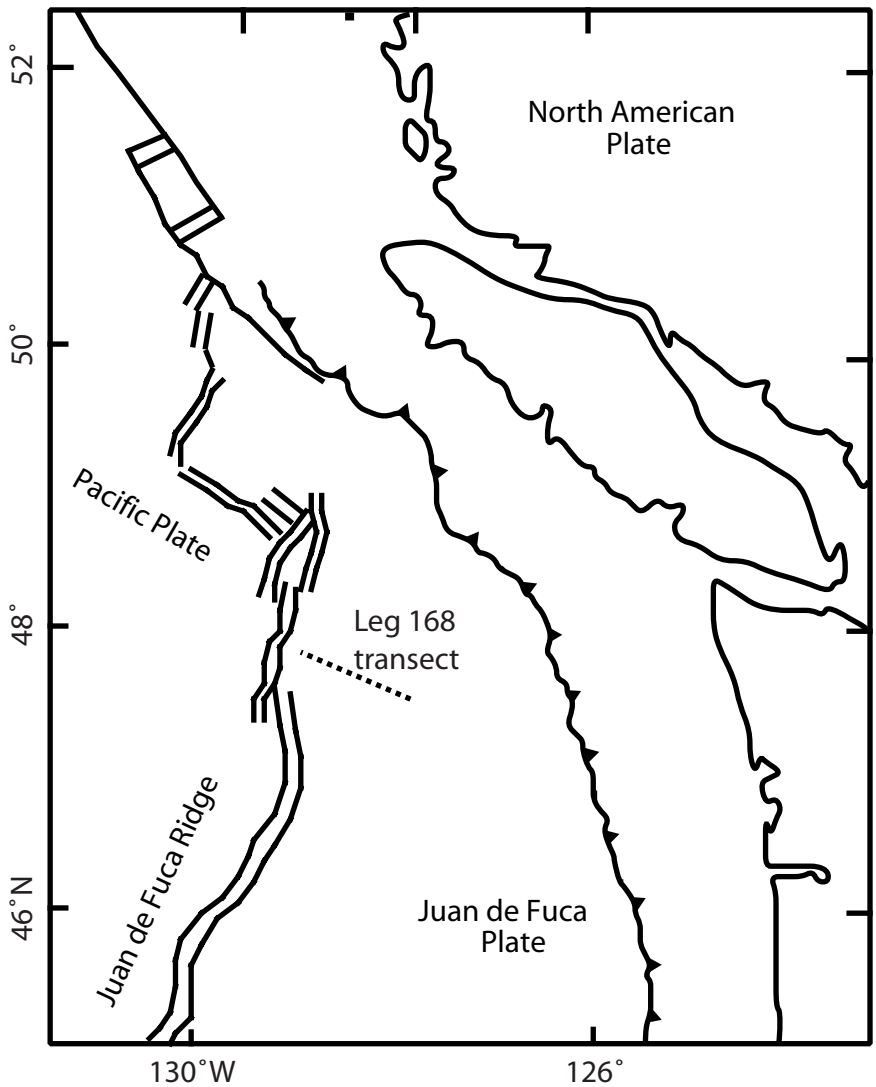

Figure 1. Site map of the northern Juan de Fuca Ridge and surrounding region. Dotted line indicates location of ODP Leg 168 transect.

best-studied examples of lateral hydrothermal circulation on a mid-ocean ridge flank [*Davis et al.*, 1989, 1997b; *Davis and Lister*, 1977; *Elderfield et al.*, 1999]. In this setting very young (<1 Ma to 3.6 Ma) crust is covered by hemipelagic mud and Pleistocene turbidites, with most of the latter shed off the North American continental margin when sea level was lower. The combination of high heat supply from the young cooling lithosphere and low-permeability sediments results in vigorous hydrothermal circulation within basement that is largely isolated from the overlying ocean. Detailed surveys show that heat flow is greatly reduced near the point of sediment onlap close to the spreading center and gradually increases to the east. Hydrothermal discharge has been observed at several locations along the ridge flank, including warm springs discovered on a basement outcrop nearly 100 km east of the ridge axis [*Becker et al.*, 2000; *Mottl et al.*, 1998], and slow upward seepage through thin and permeable sediments, inferred from pore water geochemical profiles along a buried basement ridge 40 km east of the axis [*Davis et al.*, 1997b; *Giambalvo et al.*, 2000, 2002].

[7] To investigate the nature of the hydrothermal system on the eastern flank of the Juan de Fuca

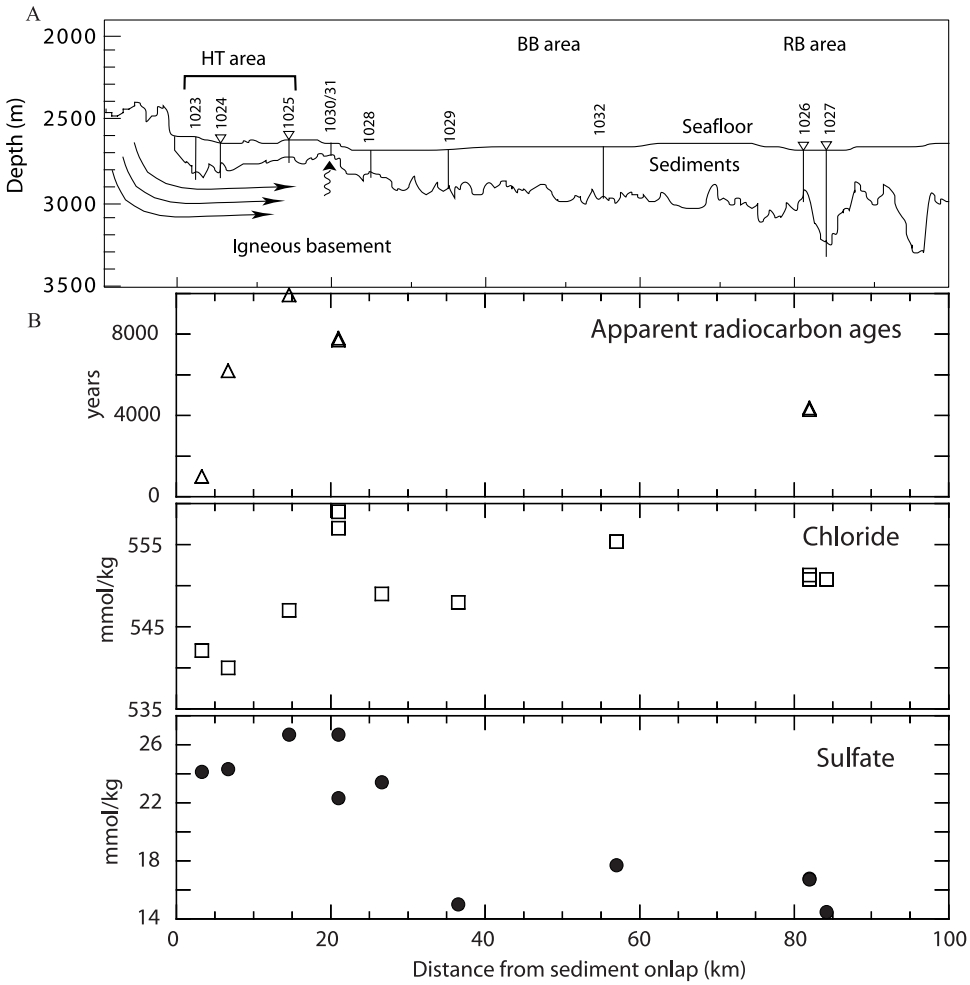

Figure 2. A. Cross-section of the Leg 168 transect showing the location of drilling sites and work areas. Inverted triangles on seafloor indicate location of sealed borehole observatories. B. Pore water chemistry data illustrating general aging trends of upper basement fluids [*Elderfield et al.*, 1999].

Ridge, Ocean Drilling Program (ODP) Leg 168 drilled a series of holes at ten sites along a 85 km transect perpendicular to the ridge crest (Figure 2). Measurements of formation temperatures, pressures, fluid composition, and rock alteration help to constrain the scale, rate, and driving forces of lateral flow in this setting and the physical properties of the upper oceanic crust. The Leg 168 transect was divided into three segments, each of which has distinct hydrothermal features. The Hydrothermal Transition (HT) area consists of the three westernmost sites (1023, 1024, and 1025) located near the transition from unsedimented to sedimented igneous basement. Heat flow at the western side of the HT area is about 20% of that predicted by lithospheric cooling models [*Davis et al.*, 1992, 1999]. Heat flow increases to the east until 20–25 km from the point of sediment onlap where measured heat flow generally matches predictions (Figure 3). The Buried Basement area, 40 to 100 km from the ridge crest, was drilled at five sites (1028, 1029, 1030, 1031, and 1032) to investigate an environment where sediment cover is continuous and the nearest basement outcrop is at least 20 km away (Figure 2). The Rough Basement area, 100 km east of the ridge axis, included two sites (1026 and 1027) located above a buried basement ridge and adjacent valley (Figure 2). These sites were investigated to determine the effect of basement top-

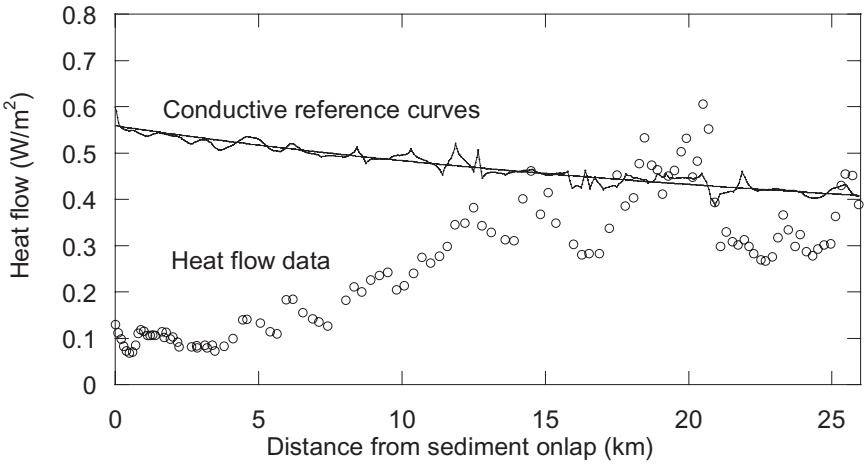

Figure 3. Heat flow data (circles) across the HT transect [*Davis et al.*, 1999]. Smooth curve is the basal heat flow boundary condition for all the models presented in this study. Irregular curve is modeled seafloor heat flow from a conductive simulation. Differences between the heat flow at the base and the seafloor result from conductive refraction caused by basement topography and varying sediment thickness.

ography and variations in sediment thickness on the driving forces and the consequences of hydrothermal circulation.

3. Lateral Flow on Ridge Flanks

[8] Several studies have interpreted regional scale heat flow patterns as resulting from large-scale lateral fluid flow. *Langseth and Herman* [1981] presented an analytic model that describes heat flow above a flat "well mixed aquifer" through which water flows laterally. This model has been applied to several ridge flank datasets, resulting in lateral specific discharge estimates of <1 to 6 m/yr [*Baker et al.*, 1991; *Fisher et al.*, 2001; *Langseth et al.*, 1992; *Langseth and Herman*, 1981].

[9] *Davis et al.* [1999] ran a series of two dimensional numerical models of lateral flow, based on observed seafloor and basement topography, to simulate the thermal effects of lateral flow and vertical mixing within the HT area of the ODP Leg 168 transect. Lateral flow was simulated by forcing cool seawater through a 600 m-thick basement layer. Vertical mixing was represented by elevating the thermal conductivity of the flow layer, effectively increasing the Nusselt number (total heat transported/transported heat in the absence of convection). Matching observed seafloor heat flow data required a lateral specific discharge (volume flux/area) of 0.3–0.9 m/yr, if there was no increase in the Nusselt number; a Nusselt number >250 if there was no lateral flow; or a combination of a lower Nusselt number and a greater specific discharge.

[10] *Elderfield et al.* [1999] presented three chemical models used to estimate lateral flow rates across the entire Leg 168 transect (~85 km). Lateral patterns in pore water concentrations of sulfate, chloride, and radiocarbon suggested average lateral velocities of 1 to 4 m/yr, equivalent to specific discharges of 0.01–0.4 m/yr, assuming effective porosity (that through which most of the flow occurs) in basement of 1–10%.

[11] The well mixed aquifer model was extended by *Rosenberg et al.* [2000] to include a flow layer below uppermost basement. This study demonstrated that flow within deeper layers extracts more heat for a given fluid flux, but that local convection within the flow layer can reduce the efficiency of large-scale lateral heat transport and extraction. For application to the HT area on the flank of the Juan de Fuca Ridge, specific discharge values on the order of 1–4 m/yr were required by the original model, with the hydrothermal layer located immediately below the sediment-basement contact, but

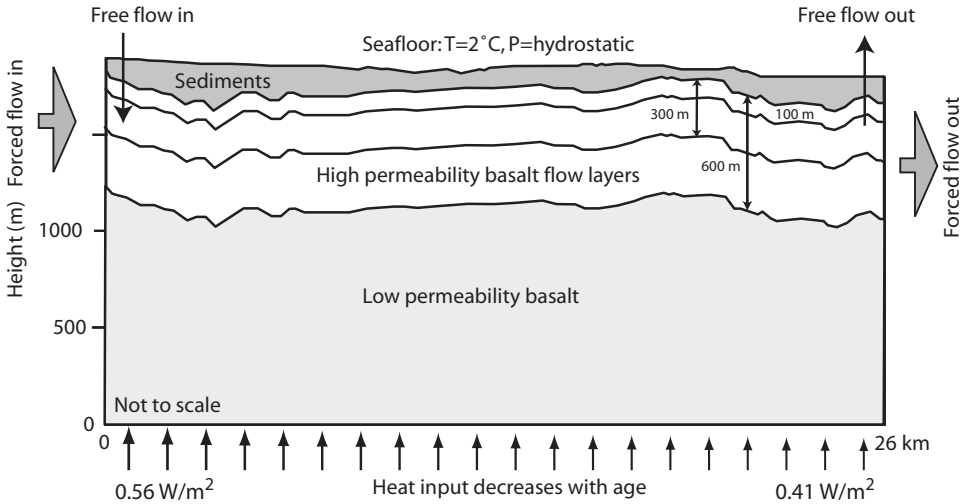

Figure 4. Numerical model domain for lateral flow models. Water enters the left and exits the right at the side (forced flow) or at the seafloor (free flow). High permeability layers 100, 300, and 600 m thick were tested. Flow rates (forced flow) or flow layer permeability (free flow) were adjusted until seafloor heat flow data were matched by the model.

values 10× lower are consistent with observations if the hydrothermal layer begins at a depth of 500 m into basement.

[12] Another indication of hydrogeologic conditions on the east flank of the Juan de Fuca Ridge comes from observations made in open and sealed borehole observatories. Borehole aquifer tests indicate that permeability in uppermost basement along the HT transect is on the order of 10^{-10} m^2, and higher values are suggested by analysis of formation pressure response to tidal perturbations [*Becker and Fisher*, 2000; *Davis et al.*, 2000]. Lateral pressure gradients across the HT area appear to be extremely small, and this also implies very high formation permeability since the fluid fluxes are relatively large [*Davis and Becker*, 1998, 2003].

[13] Although conditions interpreted on the basis of thermal and pressure observations, chemical tracers, and coupled models seem to be broadly consistent, there are important questions that remain to be resolved. How does the thickness of layers through which most of the fluid flows influence thermal and chemical estimates of flow rates? Is it possible for lateral flow to occur at inferred velocities and in the inferred direction in the absence of forcing? Can a single lateral flow model reconcile all thermal, pressure, and geochemical observations?

4. New Models of Lateral Flow

[14] We used FEHM, a transient, finite element heat and mass transport code [*Zyvoloski et al.*, 1996] to simulate two-dimensional heat and fluid flow across the HT transect. Our computational grid is 26 km-long (0.8 to 1.5 Ma in age), ~2 km-high and was constructed using seismic reflection profiles [*Davis et al.*, 1997a] that provide seafloor bathymetry and sediment thickness along the transect (Figure 4). The primary parameters that distinguish rock types are permeability, thermal conductivity, and porosity. We assign rock properties to the layers to simulate sediment, high-permeability basalt (the flow layer; 100, 300, or 600 m thick) and low-permeability basalt (Table 1). Fluid properties (density, viscosity, and enthalpy) are defined as functions of temperature and pressure [*Harvey et al.*, 1997].

4.1. Conductive Simulations

[15] We ran a conductive (no fluid flow) simulation to assess how much of the observed heat flow variability results from conductive refraction due to basement and seafloor relief. The boundary con-

Table 1. FEHM Model Parameter Values

	Lower Basalt	Basalt Flow Layer	Sediments
Thermal conductivity, W/m °C	2	2	1.2
Permeability, m^2	10^{-17}	10^{-9}–10^{-13}	10^{-17}
Rock density, kg/m^3	2700	2700	2700
Rock specific heat, J/kg °C	800	800	800
Total porosity	0.1	0.1	0.5

ditions for the conductive run included heat flow at the base of the domain calculated as a function of crustal age [*Parsons and Sclater*, 1977; *Stein and Stein*, 1994]: $HF[mW/m^2] = 500[mW]/\sqrt{age[m.y]}$, constant temperature at the seafloor (2°C), and no-flow side boundaries. Figure 3 shows the resulting seafloor heat flow pattern. Conductive refraction explains local heat flow variations as high as 50 mW/m^2 (~10% of lithospheric input), but cannot account for the large-scale heat flow depression close to the spreading center or the overall trend in rising heat flow toward the east. This analysis also suggests that conductive refraction cannot explain the area of low heat flow east of the buried ridge, 21–25 km from the point of sediment onlap.

4.2. Forced Flow Simulations

[16] We ran a set of forced flow simulations that prescribed a net lateral flow rate through the domain. These simulations were intended to quantify the lateral fluxes required to match thermal observations, to test whether there is a linear relation between the thickness of the lateral flow layer and the necessary lateral flux (as suggested by analytical models), and to evaluate the potential importance of mixed convection (convection with a net lateral flow). We added a hydrostatic seafloor boundary condition (varies with water depth), then forced 2°C water into the domain on the left side of the high permeability basalt layer and warm water (outflow temperature was not prescribed) out the right side at an equal rate (Figure 4). We adjusted the lateral flow rate until the simulated, steady state heat flow at the seafloor was close to observations, as determined by visual inspection.

[17] Figure 5 shows heat flow data, the heat input at the base of the model, and simulated heat flow for forced flow through different layer thicknesses at different specific discharges. To choose the best fitting heat flow profiles we matched the heat flow data up to ~20 km from the point of sediment onlap where model results meet the heat input at the base. We chose this point because the regional heat flow dataset suggests that this is how far the heat flow deficit extends, and pore water chemistry from the buried basement ridge (Sites 1030/31) suggests that this ridge may host a distinct flow system [*Davis et al.*, 1997b; *Elderfield et al.*, 1999]. The range of specific discharges that best fit the data are 1–2, 5–8, and 21–40 m/yr for layer thicknesses of 600, 300, and 100 m, respectively. Because the flow is forced, the model results are not sensitive to the permeability of the flow layer as long as it is low enough so that fluids in the layer do not convect during lateral flow. All models underestimated heat flow nearest the point of sediment onlap. This mismatch could be explained if water in the natural system enters the crust at a point farther west than represented by the start of our model domain. If so, higher specific discharges would be required to match heat flow farther to the east. The lateral specific discharges required to match heat flow are not linearly proportional to layer thickness, in contrast to predictions based on analytical calculations. The total amount of heat carried laterally is proportional to the lateral flux of water and its change in temperature. Thus for a given specific discharge, flow in a thinner and shallower layer transports less heat because (1) the mass flux is lower and (2) flow in a shallower layer experiences a smaller temperature contrast between inflow and outflow [*Langseth and Herman*, 1981; *Rosenberg et al.*, 2000].

[18] Modeled seafloor heat flow east of the buried ridge, 21–25 km from the point of sediment onlap, was found to match observations fairly well in several forced-flow simulations (Figure 5). This suggests that lateral fluid flow originating at the basement outcrop to the west could be responsible for heat flow suppression east of the buried ridge. It is not clear how this large-scale lateral flow relates to the deeper-seated, higher-temperature flow responsible for seafloor seepage of hydrothermally reacted fluids at ~2 mm/yr at Sites 1030 and 1031.

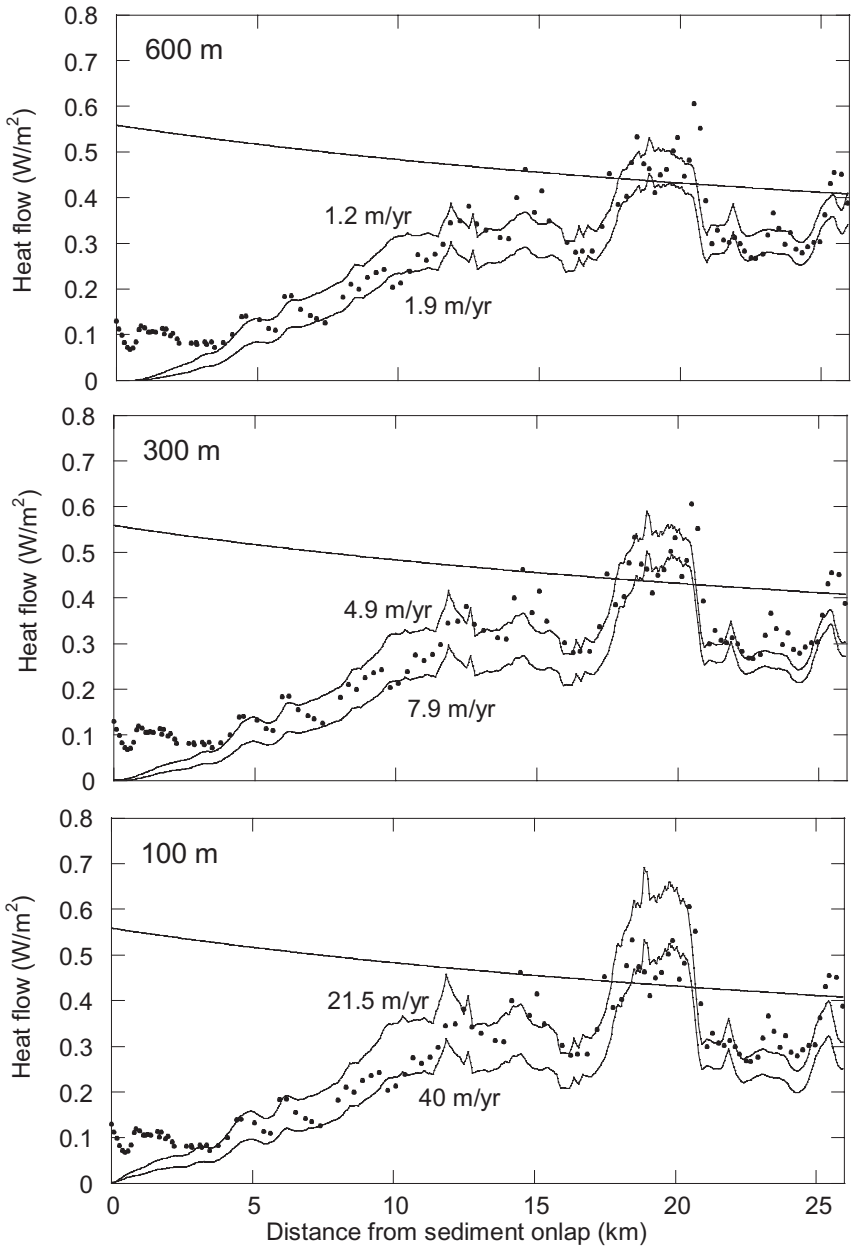

Figure 5. Best fitting model heat flow results from the forced flow models (lines) compared to observations (dots). Two specific discharges that bracket heat flow values are shown for each layer thickness. Note that as the layer becomes thinner, faster flow is required to match observations.

[19] We investigated the influence of mixed convection within the lateral flow layer during forced lateral flow by increasing the permeability of the layer and allowing fluid in it to convect. These simulations allowed us to quantify conditions under which local mixing is initiated, how mixing affects lateral flow rates required to match seafloor heat flow, and how well a high-Nusselt number approximation simulates hydrodynamic mixing.

[20] The tendency of a porous system heated from below to convect can be estimated from the Rayleigh number:

$$Ra = \frac{\alpha g k H \Delta T}{\nu \kappa_m} \quad (1)$$

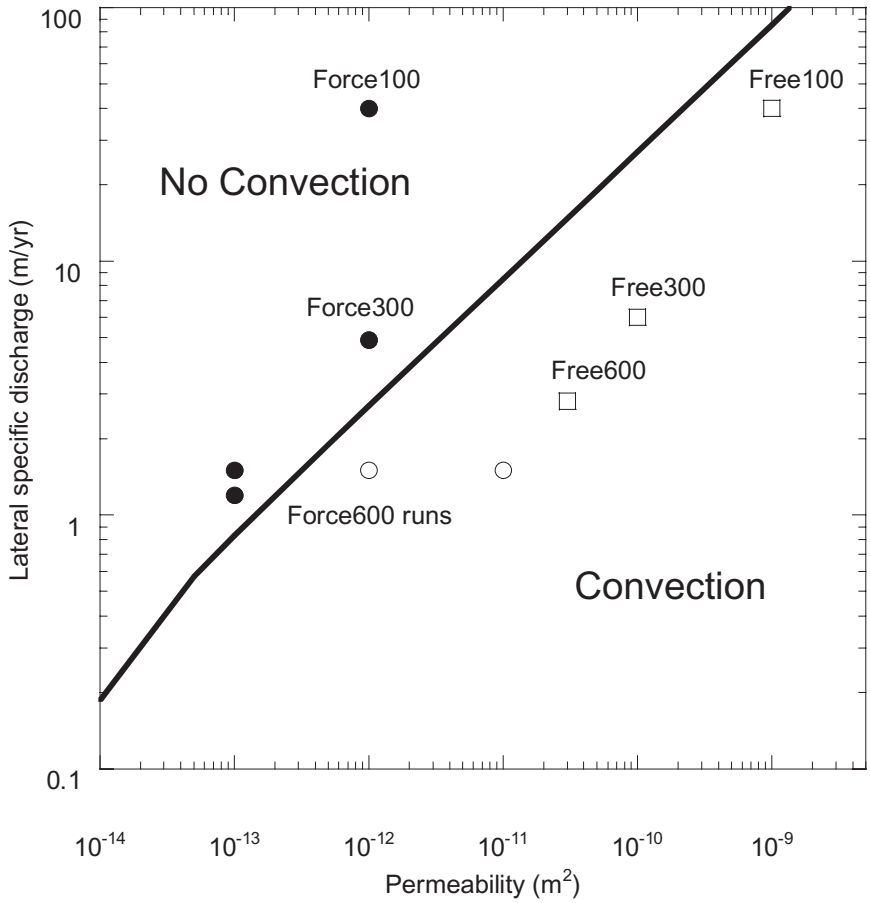

Figure 6. Cross plot of lateral specific discharge versus permeability. The solid line, defined by equations 1–3, divides conditions dominated by convection from those dominated by lateral flow. Simulations discussed in the paper are divided into forced flow (circles) and free flow (squares). Solid symbols are used if the fluids convected in the simulation.

where α is fluid expansivity, g is gravitational acceleration, k is permeability (isotropic and homogeneous), H is the thickness of the porous layer, ΔT is the vertical temperature difference across the layer, ν is kinematic viscosity, and κ_m is the thermal diffusivity of the saturated medium. Convection occurs when the Rayleigh number rises above a critical value, Ra_c, the magnitude of which depends on boundary conditions [*Nield*, 1968].

[21] Lateral flow within a layer tends to counteract buoyancy forces and results in a higher critical Rayleigh number [*Gebhart et al.*, 1988]. Laboratory studies of horizontal mixed convection (natural convection with net lateral flow) have found that the critical Rayleigh number can be estimated as [*Nield and Bejan*, 1999]:

$$Ra_c = 12 + Pe^{2/5} \tag{2}$$

where Pe is the Peclet number, a measure of the ratio of the rate of advection to conduction:

$$Pe = \frac{qH}{\kappa_m} \tag{3}$$

where q is the lateral specific discharge. Equations (1)–(3) define the critical Rayleigh number, and thus basement permeability, necessary to allow local convection in the presence of lateral flow. These calculations result in delineation of permeability and specific discharge values that separate systems dominated by local convection from those dominated by lateral flow (Figure 6). Our initial forced flow simulations plot in the "no convection" field because we assigned crustal permeability values sufficiently low so as to restrict local convection.

[22] To test the influence of increasing permeability within the flow layer on heat flow sup-

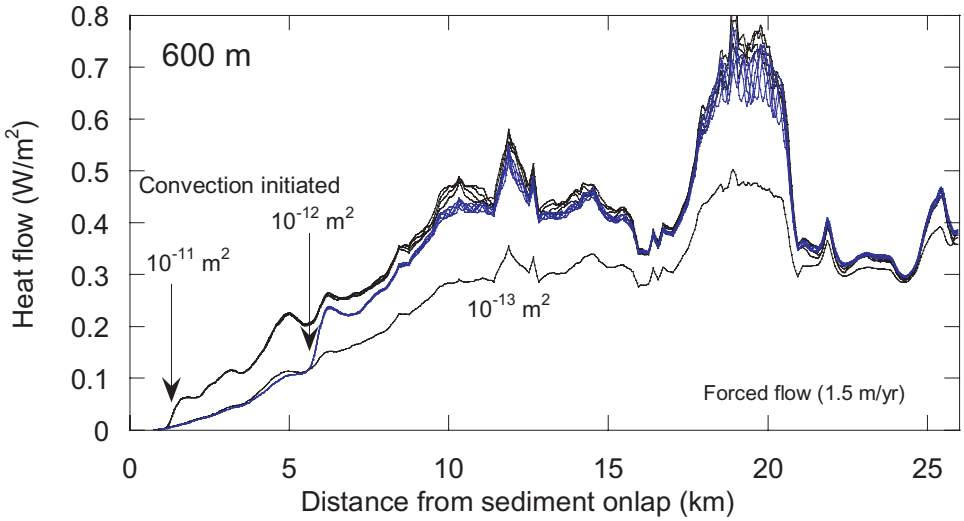

Figure 7. Plot of modeled heat flow results from the 600 m thick forced flow simulations in which we changed the permeability of the flow layer to test how convection affected modeled heat flow. Arrows show where convection was initiated. Heat flow became time dependent for the high permeability cases (10^{-12} and 10^{-11} m^2); we show four heat flow profiles for each of these to illustrate the range over which heat flow changes.

pression, we ran additional simulations for the 600-m-thick layer. We forced a net lateral specific discharge of 1.5 m/yr through layers with permeabilities of 10^{-12} and 10^{-11} m^2 and compared the results with the original forced flow in which convection was not permitted (permeability of 10^{-13} m^2) (Figure 7). At permeabilities of 10^{-12} and 10^{-11} m^2, mixed convection occurred in the parts of the system where temperatures were highest, increasing seafloor heat flow above the convecting regions. Individual circulation cells moved in the same direction as the net lateral flow and resulted in a time-dependent seafloor heat flow pattern (Figure 7). If we assume a layer permeability of 10^{-11} m^2, lateral specific discharge must increase to 2.8 m/yr in order to match heat flow observations, because of the reduced efficiency of large-scale lateral heat transport caused by local convective mixing. A similar increase in lateral flow rate was required to match heat flow observations when local convection was approximated by elevating the Nusselt number [*Davis et al.*, 1999]. Mixed convection in our simulations is somewhat more complex than represented by this approximation, since convection in the flow layer varies with location and is time-dependent, but the net thermal impact is comparable.

4.3. Free Flow Simulations

[23] While forced flow simulations allow us to test model sensitivity to specific parameters (layer thickness, specific discharge, etc.), they do not explain how flow is sustained along the HT transect. We ran a series of free flow (nonforced) simulations with conductive and hydrostatic initial conditions, as are typically used in transient models of seafloor hydrothermal circulation on ridge flanks [e.g., *Fehn and Cathles*, 1979; *Fisher et al.*, 1990; *Yang et al.*, 1996]. Fluid was allowed to enter or exit the model domain through columns of elements on the left and right side of the grids. These columns were assigned a permeability equal to that in uppermost (most permeable) basement. We believe that fluid enters basement through basalt exposed at the seafloor west of the Leg 168 transect, but the exit point for this fluid from the crust remains uncertain [*Davis et al.*, 1999].

[24] A small amount of fluid exits the seafloor as slow seepage at ODP Sites 1030 and 1031 [*Davis et al.*, 1997b; *Giambalvo et al.*, 2000, 2002], and a greater quantity of fluid vents and discharges diffusively at basement outcrops another 65 km to the east [*Mottl et al.*, 1998; *Thomson et al.*, 1995], but these fluid fluxes are small relative to

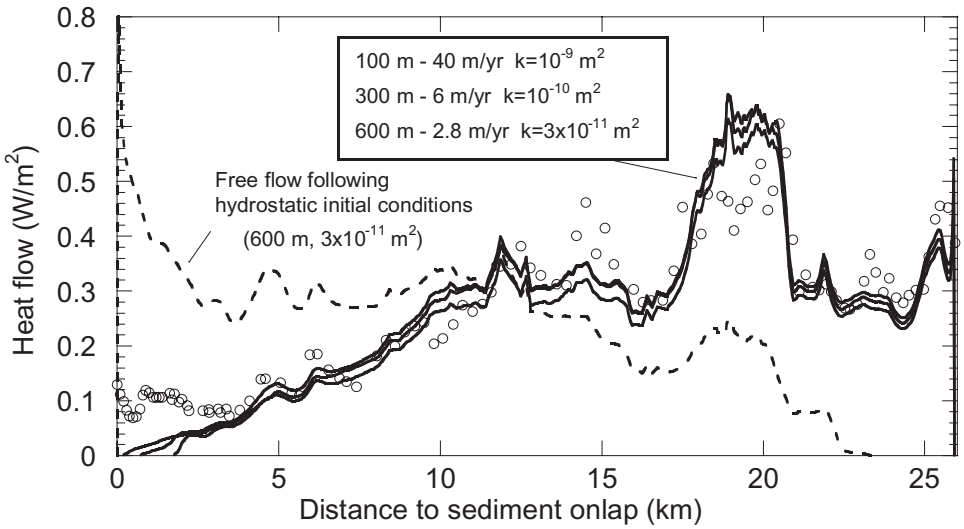

Figure 8. Modeled heat flow from free flow simulations (solid lines) can be made to match heat flow observations (circles) through adjustment of basement permeability. Dashed line is the heat flow from a simulation that used hydrostatic and conductive initial conditions, resulting in flow toward the ridge, east to west, a direction opposite to that indicated by seafloor heat flow observations.

those necessary to suppress heat flow along the HT transect. In addition, geochemical evidence suggests that the fluids exiting the seafloor at Sites 1030 and 1031 and at the outcrops to the east are distinct from those flowing laterally across the HT area [*Davis et al.*, 1997b; *Elderfield et al.*, 1999; *Mottl et al.*, 1998; *Wheat et al.*, 2000].

[25] In the absence of direct observations of focused discharge associated with lateral flow across the HT area, we created a region within which fluid was allowed to flow into or out of the model domain on the right side of the grid. Some flow within the natural system may actually move north or south, out of the plane of the models. The region through which fluids enter or exit the models on the right side of the grid should be considered simply as a high-permeability conduit that links basement to the seafloor, somewhere east of the HT transect. The free flow simulations are not intended to address the geological nature of fluid entry and exit points, but are used to assess conditions in basement between areas of recharge and discharge. One can consider this approach to be that of proxy modeling, for example, using a high Nusselt number approximation to simulate the influence of convection. We represent the influence of fluid venting to the overlying ocean by inserting a high-permeability connection that bypasses the sediments, because the actual flow geometry and vent location are not known.

[26] When the free flow models were initialized with hydrostatic and conductive initial conditions, water flowed laterally toward the ridge axis, from east (right) to west (left), in the direction opposite to that inferred from thermal and chemical data (Figure 8). The inferred direction of fluid flow is consistent with heat flow at the base of the models varying with lithospheric age and being higher on the west side of the grids than on the east side (Figure 3).

[27] We explored whether it was possible to initiate sustained fluid flow in the direction inferred from thermal observations, west to east. To start water flowing away from the ridge, we used the results of a forced flow simulation to create a "hydrothermal siphon." In the forced-flow simulations, we injected cold seawater into basement near the ridge (left side) while pumping warm water out the right side (Figure 4). The cold recharge column is denser than the warm discharge column, resulting in a lateral pressure gradient in upper basement. This pressure gradient is superimposed on that created by fluid pumping. When we restarted the simulation with no pumping, the thermally generated

pressure gradient continued to drive fluid away from the ridge as long as recharge was rapid enough to maintain cool conditions in the recharge zone, despite the greater heat input at the base of the model near the ridge. The boundary conditions were the same as in the forced-flow simulations, except that we allowed the temperature of the discharge conduit at the seafloor to adjust to the temperature of outflow. We then varied the permeability of the flow layer until we matched seafloor heat flow observations (Figure 8). The results of these simulations place important constraints on the basement permeability necessary to sustain lateral flow in the appropriate direction (west to east). When basement permeabilities were too low, the hydrothermal siphon could not be maintained, and the flow direction reverted to the east-to-west direction. This result illustrates a fundamental difficulty with modeling of these systems. Transient numerical models generally require a time-invariant geometry (the grid) and geologically reasonable initial conditions. Circulation in the natural system evolves over time as new crust is formed and moves off axis, accumulating sediment and changing in geometry and properties as the medium is modified through reactions and tectonic activity. Geologically reasonable initial conditions for models of these systems ideally should be based on observations, but generally these are not available. In the present study, the initial condition with recharge to the west is well-constrained by thermal and chemical data, but for other systems the flow direction may not be known in advance; the model then can not be used to predict a flow direction. In addition, application of steady state models or static consideration of pressure conditions may produce misleading results with regard to flow directions, since these approaches are not dependent (in a geological sense) on initial conditions.

[28] The range of permeabilities required for west to east transport in these free-flow simulations (3×10^{-11} to 10^{-9} m^2) is consistent with in situ permeability measurements [*Becker*, 2003; *Becker and Fisher*, 2000; *Fisher et al.*, 1997] and estimates based on sealed borehole observations [*Davis and Becker*, 1998, 2002, 2003]. Rates of specific discharge vary from 2.8 to 40 m/yr depending on layer thickness, a range overlapping with those inferred from forced flow simulations, but generally somewhat greater. The finding that flow direction in transient simulations depends on initial conditions suggests that caution must be applied in using computer models alone (either transient or steady state) to characterize the flow direction within natural ridge-flank, hydrothermal systems.

[29] We used results of free flow simulations to calculate deviations from hydrostatic pressures throughout the model domain. At each node, we compared the absolute pressure predicted by the model to that calculated by bootstrapping temperature-dependent fluid density from the seafloor to the depth of interest, approximating thermally ambient hydrostatic conditions. Figure 9 shows the relative pressures at the top of the flow layer across the model domain for free flow simulations. We show a range of pressures for each simulation because the free flow models include unstable convection in which cells form and migrate in the same direction as net transport. Thus the pressures measured at any one point do not reach a single steady state value, but oscillate around a mean value with an amplitude that varies with layer thickness and permeability. This finding is in general agreement with observations from long-term observatories in this region [*Davis and Becker*, 1998, 2002, 2003; *Davis et al.*, 2000] and helps to explain why pressures in sealed systems may never achieve complete stability. The greatest modeled overpressures were generated in upper basement within the buried ridge below ODP Sites 1030 and 1031. The magnitude of the predicted overpressure, 3–4 kPa, is in good agreement with that estimated by *Giambalvo et al.* [2000] based on chemically inferred seepage rates and laboratory measurements of sediment permeability ($\leq$5 kPa). The greatest predicted underpressures are found 4 km east of the point at which water enters the basement aquifer (−2 to −10 kPa), and 3–6 km east of the 1030/1031 basement ridge (−8 to −18 kPa).

[30] This pattern of elevated fluid pressures in basement ridges and lower pressures below adja-

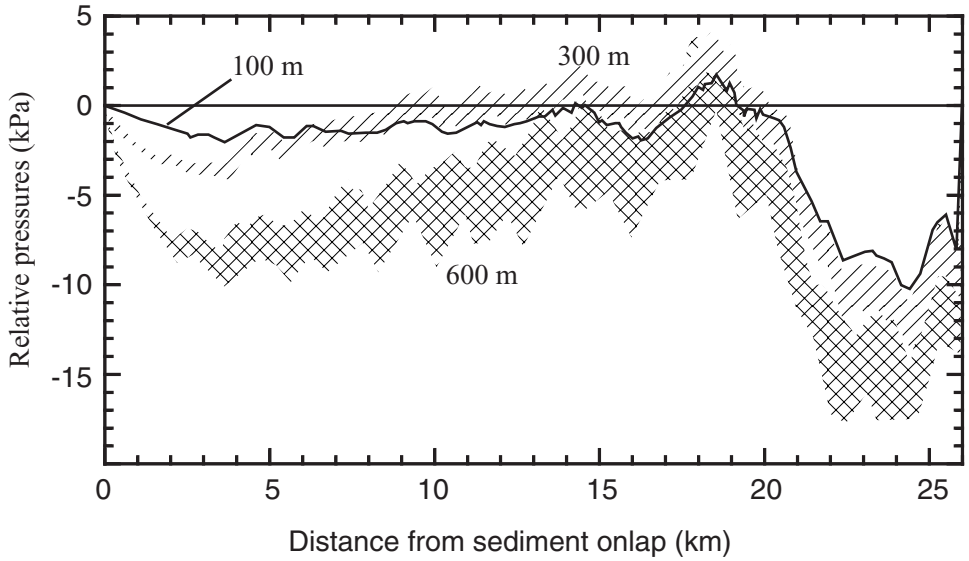

Figure 9. Relative pressures at the top of the lateral flow layer for free flow simulations. Negative values indicate downward driving forces relative to the seafloor, and positive values represent upward forces. The maximum upward driving force (~4 kPa) is located over the Site 1030/31 basement ridge where upward seepage has been observed.

cent basement troughs has been seen in other modeling and observational studies [*Davis et al.*, 1997c; *Fisher et al.*, 1994, 1990; *Wang et al.*, 1997] and is a natural consequence of basement relief and heating from below. The models predict basement underpressures at ODP Site 1024 and overpressures (in the case of a 300-m-thick lateral flow layer) at ODP Site 1025, in agreement with inferred directions of fluid flow from basement immediately prior to installation of long-term observatories [*Davis and Becker*, 2002; *Davis et al.*, 2000].

[31] It is curious that the free-flow simulations with a 300-m-thick flow layer result in a larger region having fluid overpressures than do simulations with either 100 m or 600 m layers (Figure 9). This may result from the trade-off between the increased efficiency of lateral flow within a thicker layer (allowing a lower permeability to match thermal observations, and thus generation of larger lateral pressure gradients), and the increased vigor of local convection in a thicker layer (resulting in higher temperatures in the layer). These results also demonstrate that, within a very permeable system having low pressure gradients, it is probably not wise to "calibrate" basement permeability and lateral-flow layer thickness through matching of relative basement pressures. The models suggest that pressure conditions are highly sensitive to these parameters, as well as to subtleties of basement aquifer geometry and thermal properties, and additional field and modeling constraints are needed to interpret observed pressure conditions.

5. Discussion: Physical and Chemical Constraints on Lateral Flow Rates

[32] Are thermal, pressure, and geochemical observations on the eastern flank of the Juan de Fuca Ridge consistent with a single, lateral-flow model? Our model results suggest that the thermal effects of lateral flow depend on a combination of lateral specific discharge, layer thickness, and permeability. Using a forced flow approach, we fit the heat flow observations with specific discharges of 1.2 to 40 m/yr. Free flow models suggest an overlapping range of lateral specific discharges (2.8 to 40 m/yr), and the occurrence of mixed convection within the flow layer. To compare model-derived specific discharges to lateral flow velocities based on chemical data we need to calculate equivalent average lateral velocities (specific discharge/effective porosity). Since effective porosity is difficult to measure, we consider a range of values (1–

10%), resulting in average lateral velocities of 12 to 4000 m/yr.

5.1. Reconciling Chemical and Physical Models

[33] Apparent ^{14}C ages increase across the HT area with distance from the sediment onlap, 1000, 6210, and 9930 years for Sites 1023, 1024, and 1025, respectively [*Elderfield et al.*, 1999]. Lateral velocities estimated from these ages and the distances from these sites to the point of sediment onlap, based on a piston-flow model, are 1.1 to 3.3 m/yr [*Elderfield et al.*, 1999]. Similar velocities were estimated based on Cl and SO_4 analyses of pore fluids, and associated models of solute transport involving changing boundary conditions (for Cl) and reaction (for SO_4). These velocities are considerably slower than the range based on coupled heat and fluid flow models (12 to 4000 m/yr).

[34] A piston-flow interpretation of radiocarbon transport is based on the assumption that the only sink for radiocarbon is radioactive decay. This approach neglects both diffusive losses to surrounding, hydrologically inactive regions and mixing within zones in which flow is concentrated. Even in the case of nonreactive tracers, apparent groundwater age increases more rapidly than indicated by the time elapsed since recharge because of the loss of "age-mass" [*Bethke and Johnson*, 2002; *Goode*, 1996]. The actual fluid velocity determined on the basis of geochemical tracers, within an aquifer system at steady state that contains regions in which no flow occurs (confining layers), may be calculated as

$$v_x = \left[\frac{(1+F)\Delta x}{\Delta \tau}\right] \quad (4)$$

where $F = (n_{con}b_{con})/(n_{aq}b_{aq})$, n = porosity, b = layer thickness, subscripts *aq* and *con* refer to the aquifer and confining layer, respectively, Δx is the lateral spacing between sample locations, and $\Delta\tau$ is the apparent age difference between fluids at each location [*Bethke and Johnson*, 2002].

[35] It seems surprising at first that equation (4) does not include any dependence on values of dispersion or fluid velocity, but this arises because, after a sufficiently long time following recharge, the flux of age-mass from the primary flow channel into more stagnant areas reaches steady state [*Bethke and Johnson*, 2002]. An appropriate analogy in heat flow is that a steady state thermal gradient between fixed-boundary temperatures is not affected by the value of thermal conductivity between the boundaries. Thermal conductivity affects how quickly steady state is achieved and how large the flux is in the presence of a particular gradient, but not the absolute temperature at any point. In the case of younger fluid flowing rapidly between regions containing much older fluid, age-mass reaches steady state when age-mass movement between these regions balances the loss of age-mass associated with flow in the primary channel. This is a good approximation when the thickness of the aquifer (the channel(s) hosting primary flow) is thin relative to the surrounding stagnant regions, a criterion that is certainly met within the upper oceanic crust, as described below. Under these conditions, the correction that must be applied to apparent ages to estimate flow velocities is based entirely on F, the ratio of the volume of water within the surrounding stagnant layers to the volume of water within the aquifer. We note that this correction applies to all kinds of heterogeneous aquifers, whether flow is dominantly through fractures or porous media. Equation (4) reduces to the piston-flow approximation if $F = 0$, in which case the actual fluid velocity is calculated as the ratio of distance to age difference.

[36] We have applied equation (4) to the HT transect to estimate corrections necessary to account for diffusive losses. If we assume reasonable values for aquifer effective porosity (1–10%), aquifer thickness (10–500 m), confining layer porosity (1–5% for underlying basement, 50–60% for overlying sediments), and confining layer thickness (1000 m for underlying basement, 200 m for overlying sediments), the appropriate correction factors for this hydrogeologic system are on the order of 2 to 50. These correction estimates are likely to be conservative because (1) the confining layer below the shallow basement aquifer is many kilometers thick (making the volume of water in the confining layer even larger than assumed), and (2) these

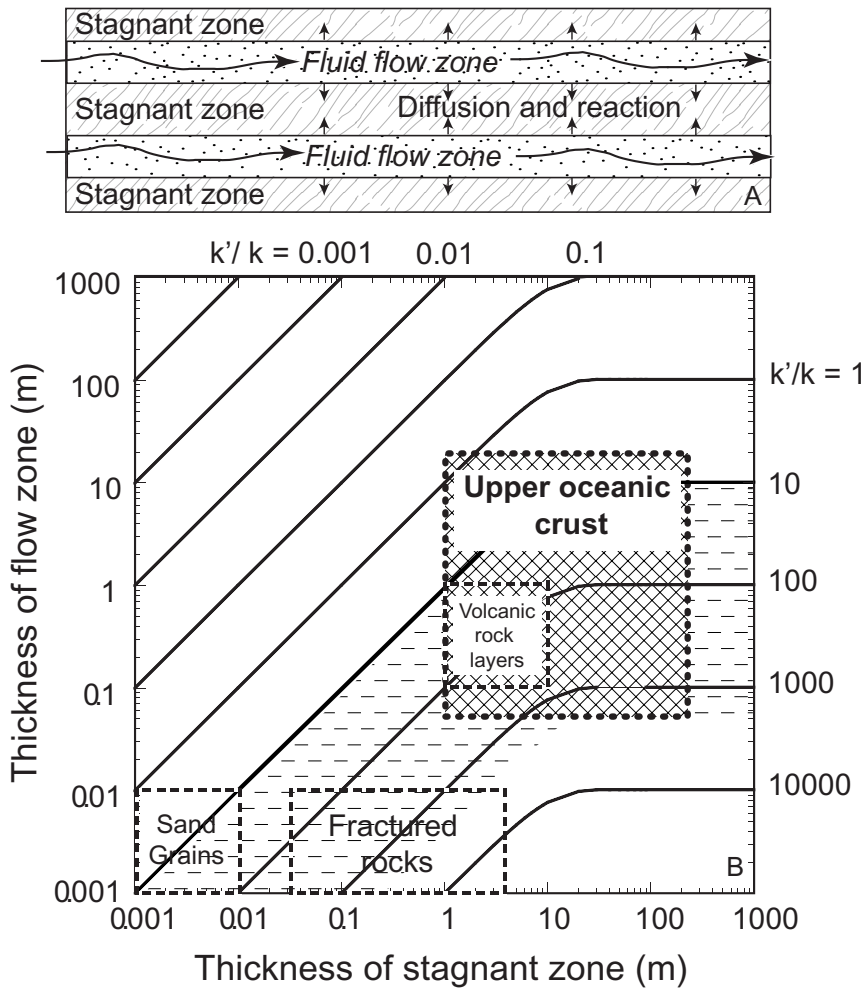

Figure 10. A. Conceptual model illustrating the diffusion and decay of ^{14}C into stagnant zones that border high permeability flow zones (modified from *Sanford* [1997]). B. Log-log plot of flow zone thickness versus stagnant zone thickness showing lines of equal k'/k values. $k'/k > 1$ represent aquifers in which diffusion provides an important sink for ^{14}C. Regions enclosed by dashed boxes represent typical aquifer materials. Cross-hatched area represents the range of k'/k values required to reconcile coupled heat and fluid models with apparent ^{14}C ages [*Elderfield et al.*, 1999]. Dotted box represents region defined by thickness of flow and stagnant zones interpreted from borehole logs from the oceanic crust (Figure 11). The correspondence of the dotted box and the shaded region suggests that diffusion-corrected (actual fluid) ^{14}C ages may be $10-1000\times$ younger than apparent ages.

calculations neglect the influence of flow channeling within the aquifer (isolation of most flow within a small fraction of the most permeable regions [e.g., *Fisher and Becker*, 2000; *Tsang and Neretnieks*, 1998]) and associated mixing.

[37] A different approach was developed for interpretation of radiocarbon ages from aquifer fluids [*Sanford*, 1997; *Sudicky and Frind*, 1981]. Fluid flow within heterogeneous aquifers is considered to be focused within regions that are surrounded by stagnant layers in which transport is dominantly diffusive (Figure 10). A stagnant zone "width factor" is defined as $w = \tanh(b\sqrt{k/D}/2)$, where b = thickness of stagnant layers, D = molecular diffusion within this zone, and k = decay constant for radiocarbon. The rate of diffusive loss is calculated as

$$k' = \left[2w\sqrt{kD}/(na)\right] \quad (5)$$

where n = aquifer porosity and a = aquifer thickness. The relative importance of diffusive to radiometric loss is expressed by the ratio k'/k. Typical values of

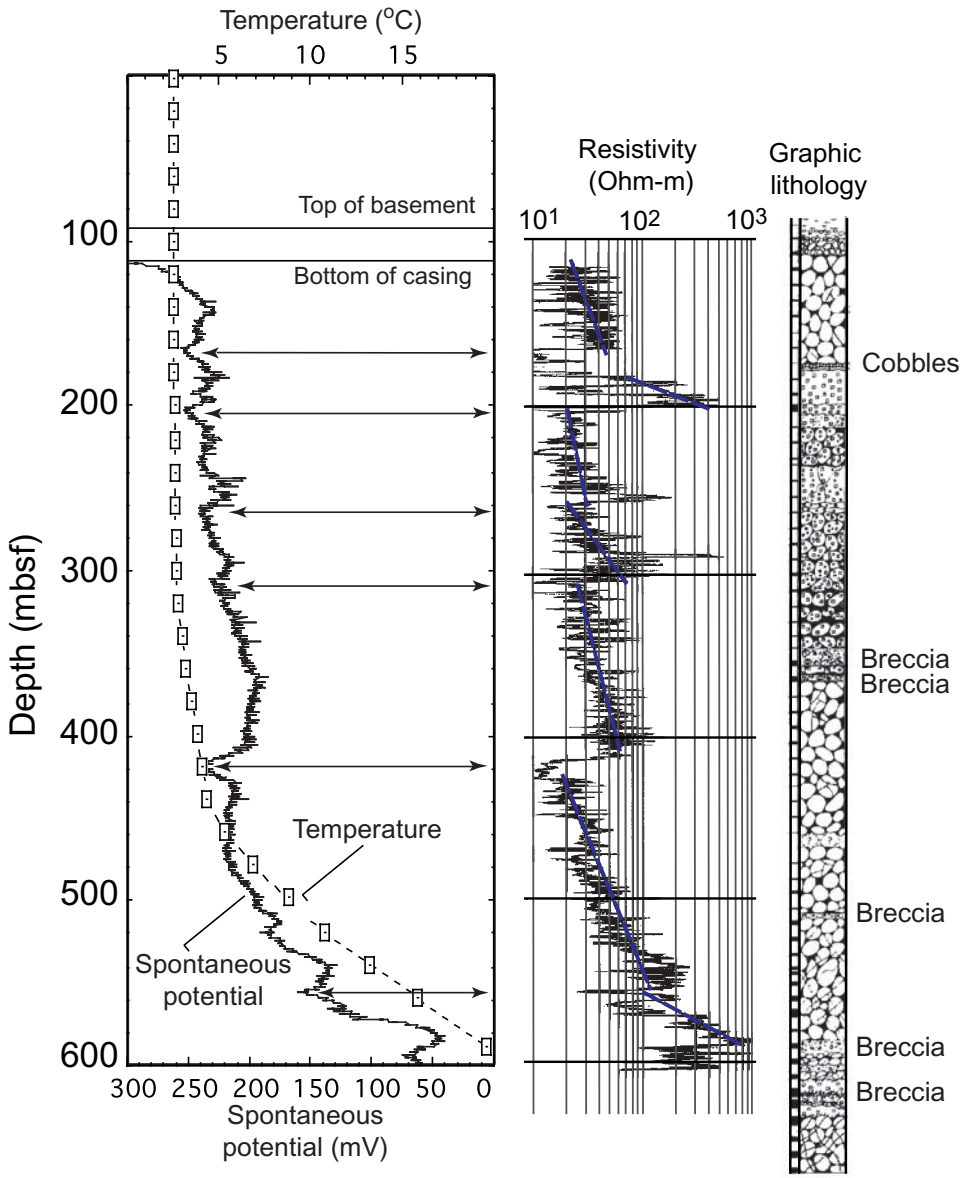

Figure 11. Logging and lithologic data from ODP Hole 395A (modified from *Bartetzko et al.* [2001], *Becker et al.* [2001], and *Fisher* [2003]). Arrows show intervals where the spontaneous potential (SP) log indicates that water is flowing into the formation. These zones correspond to the porous tops of individual volcanic flow units imaged by the resistivity log and the core lithology (data from *Matthews et al.* [1984] and *Becker et al.* [1998]).

k'/k noted for "volcanic rock layers" and "fractured rocks" are on the order of 10–1000 [*Sanford*, 1997]. Corrected fluid velocities (v_x) based on radiocarbon measurements are calculated from uncorrected values as: $v_x = \frac{\Delta x}{\Delta \tau}\left(\frac{k+k'}{k}\right)$. As the value of k' increases, the correction factor goes to k'/k.

[38] Values of $k'/k > 1$ indicate significant diffusion losses and lead to underestimates of water velocities and overestimates of water ages. Based on average lateral velocities estimated from the thermal models (12 to 4000 m/yr), we calculated a range of modeled water ages for each of the HT sites (Site 1023:1–200 yrs, Site 1024: 2–450 yrs, Site 1025: 4–1000 yrs). These model ages correspond to a k'/k range of 10 to 2500, as appropriate for volcanic and fractured aquifers (Figure 10).

[39] There are additional indications that even these large corrections may be conservative. In

kilometer-scale tracer studies of matrix diffusion within a fractured granite aquifer system, effective rock matrix diffusivity has been shown to be at least 3×10^{-8} m^2/s, a full order of magnitude greater than the known free-water diffusivity [*Becker and Shapiro*, 2000; *Shapiro*, 2001]. This result contrasts with the standard model for diffusive transport within a porous medium, in which the effective diffusivity is lower than that for free water, often by an order of magnitude or more. The documented range in fracture transmissivity at the field site is six orders of magnitude, and the high effective diffusivity is thought to result from preferential migration of tracer along the most permeable fractures, which are generally well-connected over relatively short distances [*Shapiro and Hsieh*, 1998]. If the effective diffusivity of geochemical tracers in ridge flank hydrothermal circulation systems is also greater than the free water value, then the diffusive loss correction that needs to be applied to ^{14}C data would result in k'/k values considerably greater than 1000×, and thus fluid velocities within parts of basement that are on the order of kilometers per year or more.

[40] *Elderfield et al.* [1999] also discuss flow directions and rates in basement along the western part of the ODP Leg 168 transect based on analysis of chloride and sulfate data. These chemical constraints on rates of fluid flow across the HT sites are broadly consistent with the ^{14}C analyses, although apparent rates vary somewhat between pairs of sites and tracer systems. These differences are likely to result from uncertainties in transport and reaction rates within sediments overlying the basement aquifer, and from other complexities not represented in the conceptual models used to interpret the data. Understanding the reasons for solute patterns of individual species would require application of more sophisticated reaction path models, to take into account the many processes influencing pore fluid chemistry in this setting, and may also require consideration of across-profile (in addition to along-profile) transport. Our goal in the present study is not to reconcile interpretations based on different geochemical techniques (particularly since these differences are modest), but to reconcile the order-of-magnitude differences in apparent flow rates apparent from thermal and geochemical methods. These differences suggest something important about the nature of the ridge-flank flow system: that most of the flow occurs through a relatively small fraction of rock. In the next section, we provide a physical justification for this interpretation.

5.2. Evidence for Focused Fluid Flow in the Oceanic Cust

[41] Although we have limited borehole lithologic data from the HT area, cores and geophysical logs from other sites allow estimation of the thickness of distinct flow and stagnant zones in these areas. Lithologic and electrical resistivity logs from DSDP/ODP Hole 395A, 7 Ma seafloor on the western flank of the Mid-Atlantic Ridge, were compared by shipboard scientists after an initial phase of drilling and experiments and interpreted to indicate a series of vertically distinct, basaltic flows [*Matthews et al.*, 1984]. Each flow unit is characterized by greater electrical resistivity at the base and lower electrical resistivity at the top, thought to result from an increase in porosity in rocks deposited during the final stages of each effusive event. Temperature logs collected soon after drilling [*Becker et al.*, 1984] indicated that bottom water was being drawn down Hole 395A because the formation pressure was less than that generated by a borehole filled with cold seawater (a consequence of the drilling process).

[42] Scientists returned to Hole 395A in 1997 to conduct additional geophysical experiments, including recording of a spontaneous potential (SP) log in the open hole [*Becker and Malone*, 1998]. The SP tool is used commonly in oil wells to determine the locations of intervals within a borehole that receive or produce borehole fluid [*Goldberg*, 1997]. Deflections in the Hole 395A SP log clearly correlate with the tops of individual resistivity sequences [*Bartetzko et al.*, 2001; *Becker et al.*, 2001; *Fisher*, 2003], suggesting that these thin layers, independently interpreted based on lithologic and resistivity data to have higher porosity, are also the most hydrologically active intervals. The typical thicknesses of the most and least hydrologically active sections of this borehole are on the

order of 1–10 m and 10–100 m, respectively. Similar scales of layering, on the basis of combined geological geochemical, and geophysical observations, have been noted in numerous other DSDP and ODP drill holes [e.g., *Alt et al.*, 1996; *Bach et al.*, 2002; *Jarrard and Broglia*, 1991; *Karson*, 2002; *Langseth and Becker*, 1994; *Larson et al.*, 1993].

[43] Given typical flow zone thickness of 1–10 m and stagnant zone thickness of 10–100 m, k'/k values in upper basement of young oceanic crust are on the order of 10 to 1000 (Figure 10b), consistent with the difference between flow velocity estimates in the HT area based on thermal and chemical observations. These estimates suggest that loss of ^{14}C by diffusion could occur 10–1000× faster than by decay. If correct, lateral flow rates across the HT transect could be 10–1000× faster than indicated by piston-flow interpretations of ^{14}C data.

6. Summary and Conclusions

[44] We prepared a series of transient, coupled heat and fluid flow models of the east flank of the Juan de Fuca Ridge. Some models included forced lateral flow, with and without convection in the lateral flow layer. Other models were allowed to flow freely. Flow rates and basement permeabilities were adjusted until a match was obtained between modeled heat flow and that observed along the HT transect. Forced flow models in which convection was inhibited suggest that the relation between flow layer thickness and heat flow suppression is not linear, in contrast to results of analytical calculations. Models in which convection was allowed to occur along with forced flow confirm that local mixing reduces the efficiency of heat flow suppression. Models in which flow was allowed to occur without forcing had to be started with initial conditions generated by forced flow, in order to get fluid to flow in the direction inferred from thermal and chemical observations. These initial conditions caused the creation of a "hydrothermal siphon," in which the high density of cool, recharging fluid results in flow away from an area of higher basal heat flow. Pressure differences predicted by free flow models matched observations, including the magnitude and distribution of under- and overpressures. Flow velocities across the HT area predicted by coupled heat and fluid flow models were 10–1000× greater than those predicted by piston-flow calculations based on ^{14}C data. This difference can be reconciled through consideration of diffusional loss (large-scale dispersion) of ^{14}C to stagnant regions surrounding the primary flow layers. These results illustrate the importance of mapping out the primary flow layers in oceanic crust, and in considering reactive transport for interpreting geochemical tracers.

Acknowledgments

[45] This work would not have been possible without the expertise of the ODP Leg 168 drilling and engineering crews and the scientific party. We also thank Carl Gable, George Zyvoloski and Phil Stauffer at LANL for modeling and grid generation assistance. Thanks to Keir Becker and two anonymous reviewers for helpful suggestions that improved the manuscript. This research was supported by USSSP grants 168-F000500 and 168-F000501, CULAR (LANL/UCSC) project STB-UC98-181, and NSF project 9819242. Sandia is a multiprogram laboratory operated by Sandia Corporation, a Lockheed Martin Company, for the United States Department of Energy's National Nuclear Security Administration under contract DE-AC04-94AL85000.

References

Alt, J. C., Subseafloor processes in mid-ocean ridge hydrothermal systems, in *Seafloor Hydrothermal Systems: Physical, Chemical, Biological and Geological Interactions*, *Geophys. Monogr. Ser.*, vol. 91, edited by S. E. Humphris et al., pp. 85–114, AGU, Washington, D. C., 1995.

Alt, J. C., D. A. H. Teagle, C. Laverne, D. A. Vanko, W. Bach, J. Honnorez, K. Becker, M. Ayadi, and P. A. Pezard, Ridge-flank alteration of upper oceanic crust in the Eastern Pacific: Synthesis of results for volcanic rocks of Holes 504B and 896A, *Proc. Ocean Drill. Program Sci. Results*, *148*, 435–450, 1996.

Bach, W., S. E. Humphris, and A. T. Fisher, Fluid flow and fluid-rock interaction within oceanic crust: Reconciling geochemical, geological, and geophysical observations, in *Subseafloor Biosphere at Mid-ocean Ridges*, edited by C. Cary, E. Delong, D. Kelley, and W. S. D. Wilcock, in press, AGU, Washington, D. C., 2002.

Baker, P., P. Stout, M. Kastner, and H. Elderfield, Large-scale lateral advection of seawater through oceanic crust in the central equatorial Pacific, *Earth. Planet. Sci. Lett.*, *105*, 522–533, 1991.

Bartetzko, A., P. Pezard, D. Goldberg, Y.-F. Sun, and K. Becker, Volcanic stratigraphy of DSDP/ODP Hole 395A: An in-

terpretation using well-logging data, *Mar. Geophys. Res.*, *22*(111–127), 2001.

Becker, K., In situ determinations of the permeability of the igneous oceanic crust, in *Hydrogeology of the Oceanic Lithosphere*, edited by E. E. Davis and H. Elderfield, in press, Cambridge Univ. Press, New York, 2003.

Becker, K., and A. Fisher, Permeability of upper oceanic basement on the eastern flank of the Endeavor Ridge determined with drill-string packer experiments, *J. Geophys. Res.*, *105*(B1), 897–912, 2000.

Becker, K., and M. J. Malone, *Proceedings of the Ocean Drilling Project, Initial Reports*, vol. 174B, Ocean Drill. Program, College Station, Tex., 1998.

Becker, M. W., and A. M. Shapiro, Tracer transport in fractured crystalline rock: Evidence of nondiffusive breakthrough tailing, *Water Resour. Res.*, *36*(7), 1677–1686, 2000.

Becker, K., M. G. Langseth, and R. D. Hyndman, Temperature measurements in Hole 395A, Leg 78B, in *Initial Reports of the Deep Sea Drilling Project*, edited by R. Hyndman and M. Salisbury, pp. 689–698, U.S. Govt. Print. Off., Washington, D. C., 1984.

Becker, K., et al., *Proceedings of the Ocean Drilling Project: Initial Reports*, vol. 174B, Ocean Drill. Program, College Station, Tex., 1998.

Becker, N. C., C. G. Wheat, M. J. Mottl, J. Karsten, and E. E. Davis, A geological and geophysical investigation of Baby Bare, locus of a ridge flank hydrothermal system in the Cascadia Basin, *J. Geophys. Res.*, *105*(B10), 23,557–23,568, 2000.

Becker, K., A. Bartetzko, and E. E. Davis, Leg 174B synopsis: Revisiting Hole 395A for logging and long-term monitoring of off-axis hydrothermal processes in young oceanic crust, *Proc. Ocean Drill. Project Sci. Results*, *174B*, 1–12, 2001.

Bethke, C. M., and T. M. Johnson, Paradox of groundwater age, *Geology*, *30*(2), 107–110, 2002.

Davis, E., and K. Becker, Borehole observations record driving forces for hydrothermal circulation in young oceanic crust, *Eos Trans. AGU*, *79*(31), 369, 377–378, 1998.

Davis, E. E., and K. Becker, Observations of natural-state fluid pressures and temperatures in young oceanic crust and inferences regarding hydrothermal circulation, *Earth. Planet. Sci. Lett.*, *204*, 231–248, 2002.

Davis, E. E., and K. Becker, Observations of temperature and pressure: Constraints on ocean crustal hydrologic state, properties, and flow, in *Hydrogeology of the Oceanic Lithosphere*, edited by E. E. Davis and H. Elderfield, pp. in press, Cambridge Univ. Press, New York, 2003.

Davis, E. E., and C. R. B. Lister, Heat flow measured over the Juan de Fuca Ridge: Evidence for widespread hydrothermal circulation in a highly heat-transportive crust, *J. Geophys. Res.*, *82*, 4845–4860, 1977.

Davis, E. E., D. S. Chapman, C. Forster, and H. Villinger, Heat-flow variations correlated with buried basement topography on the Juan de Fuca Ridge flank, *Nature*, *342*, 533–537, 1989.

Davis, E. E., et al., FlankFlux: An experiment to study the nature of hydrothermal circulation in young oceanic crust, *Can. J. Earth Sci.*, *29*(5), 925–952, 1992.

Davis, E. E., D. S. Chapman, H. Villinger, S. Robinson, J. Grigel, A. Rosenberger, and D. Pribnow, Seafloor heat flow on the eastern flank of the Juan de Fuca Ridge: Data from the "FlankFlux" studies through 1995, in *Proc. Ocean Drill. Project Initial Rep.*, *168*, 23–33, 1997a.

Davis, E. E., A. T. Fisher, and J. Firth, *Proceedings of the Ocean Drilling Program, Initial Reports*, 470 pp., Ocean Drill. Program, College Station, Tex., 1997b.

Davis, E. E., K. Wang, J. He, D. S. Chapman, H. Villinger, and A. Rosenberger, An unequivocal case for high Nusselt-number hydrothermal convection in sediment-buried igneous oceanic crust, *Earth. Planet. Sci. Lett.*, *146*, 137–150, 1997c.

Davis, E. E., D. S. Chapman, K. Wang, H. Villinger, A. T. Fisher, S. W. Robinson, J. Grigel, D. Pribnow, J. Stein, and K. Becker, Regional heat-flow variations across the sedimented Juan de Fuca Ridge eastern flank: Constraints on lithospheric cooling and lateral hydrothermal heat transport, *J. Geophys. Res.*, *104*(B8), 17,675–17,688, 1999.

Davis, E. E., W. Wang, K. Becker, and R. E. Thompson, Formation-scale hydraulic and mechanical properties of oceanic crust inferred from pore-pressure response to periodic seafloor loading, *J. Geophys. Res.*, *105*(B6), 13,423–13,435, 2000.

Elderfield, H., and A. Schultz, Mid-ocean ridge hydrothermal fluxes and the chemical composition of the ocean, *Annu. Rev. Earth Planet. Sci.*, *24*, 191–224, 1996.

Elderfield, H., C. G. Wheat, M. J. Mottl, C. Monnin, and B. Spiro, Fluid and geochemical transport through oceanic crust: A transect across the eastern flank of the Juan de Fuca Ridge, *Earth. Planet. Sci. Lett.*, *172*, 151–165, 1999.

Fehn, U., and L. Cathles, Hydrothermal convection at slow-spreading midocean ridges, *Tectonophysics*, *55*, 239–260, 1979.

Fisher, A., Geophysical constraints on hydrothermal circulation: Observations and models, in *Energy and Mass Transfer in Submarine Hydrothermal Systems*, edited by P. Halbach, V. Tunnicliffe, and J. Hein, in press, Dahlem Univ. Press, Berlin, Germany, 2003.

Fisher, A., and K. Becker, Channelized fluid flow in oceanic crust reconciles heat-flow and permeability data, *Nature*, *403*, 71–74, 2000.

Fisher, A. T., K. Becker, T. N. Narasimhan, M. G. Langseth, and M. J. Mottl, Passive, off-axis convection on the southern flank of the Costa Rica Rift, *J. Geophys. Res.*, *95*, 9343–9370, 1990.

Fisher, A. T., K. Becker, and T. N. Narasimhan, Off-axis hydrothermal circulation: Parametric tests of a refined model of processes at Deep Sea Drilling Project/Ocean Drilling Program site 504, *J. Geophys. Res.*, *99*, 3097–3121, 1994.

Fisher, A. T., K. Becker, and E. E. Davis, The permeability of young oceanic crust east of Juan de Fuca Ridge determined using borehole thermal measurements, *Geophys. Res. Lett.*, *24*, 1311–1314, 1997.

Fisher, A., E. Giambalvo, J. Sclater, M. Kastner, B. Ransom, Y. Weinstein, and P. Lonsdale, Heat flow, sediment and pore fluid chemistry, and hydrothermal circulation on the east

flank of Alarcon Ridge, Gulf of California, *Earth. Planet. Sci. Lett.*, *188*, 521–534, 2001.

Gebhart, B., Y. Jaluria, R. L. Mahajan, and B. Sammakia, *Buoyancy-Induced Flows and Transport*, 971 pp., Taylor and Francis, Philadelphia, Pa., 1988.

Giambalvo, E., A. T. Fisher, L. Darty, J. T. Martin, and R. P. Lowell, Origin of elevated sediment permeability in a hydrothermal seepage zone, eastern flank of Juan de Fuca Ridge, and implications for transport of fluid and heat, *J. Geophys. Res.*, *105*(B1), 913–928, 2000.

Giambalvo, E., C. Steefel, A. Fisher, N. Rosenberg, and C. G. Wheat, Effect of fluid-sediment reaction on hydrothermal fluxes of major elements, eastern flank of the Juan de Fuca Ridge, *Geochim. Cosmochim. Acta*, *66*(10), 1739–1757, 2002.

Goldberg, D., The role of downhole measurements in marine geology and geophysics, *Rev. Geophys.*, *35*(3), 315–342, 1997.

Goode, D. J., Direct simulation of groundwater age, *Water Resour. Res.*, *32*, 289–296, 1996.

Harvey, A. H., A. P. Peskin, and S. A. Kline, *NIST/ASME Steam Properties*, 49 pp., Natl. Inst. for Stand. and Technol., Gaithersburg, Md., 1997.

Hobart, M., M. Langseth, and R. N. Anderson, A geothermal and geophysical survey of the south flank of the Costa Rica Rift, sites 504 and 505, in *Initial Reports of the Deep Sea Drilling Project*, edited by R. Anderson, J. Honnorez, and K. Becker, pp. 379–404, U.S. Govt. Print. Off., Washington, D. C., 1985.

Jarrard, R. D., and C. Broglia, Geophysical properties of oceanic crust at Sites 768 and 770, *Proc. Ocean Drill. Project Sci. Results*, *124*, 75–90, 1991.

Karson, J. A., Geologic structure of the uppermost oceanic crust created at fast- to intermediate-rate spreading centers, *Annu. Rev. Earth Planet. Sci.*, *30*, 347–384, 2002.

Langseth, M., and K. Becker, Structure of igneous basement at sites 857 and 858 based on leg 139 downhole logging, *Proc. Ocean Drill. Project Sci. Results*, *139*, 573–583, 1994.

Langseth, M. G., and B. Herman, Heat transfer in the oceanic crust of the Brazil Basin, *J. Geophys. Res.*, *86*, 10,805–10,819, 1981.

Langseth, M. G., J. Cann, J. Natland, and M. Hobart, Geothermal phenomena at the Costa Rica Rift, background to objectives for drilling at Deep Sea Drilling Project sites 501, 504, 505, in *Initial Reports, Deep Sea Drilling Project*, vol. 69, edited by J. R. Cann et al., pp. 5–29, U.S. Govt. Print. Off., Washington, D. C., 1983.

Langseth, M. G., R. D. Hyndman, K. Becker, S. H. Hickman, and M. H. Salisbury, The hydrogeological regime of isolated sediment ponds in mid-oceanic ridges, in *Initial Reports, Deep Sea Drilling Project*, vol. 78, edited by R. H. Hyndman and M. H. Salisbury, pp. 825–837, U.S. Govt. Print. Off., Washington, D. C., 1984.

Langseth, M. G., K. Becker, R. P. Von Herzen, and P. Schultheiss, Heat and fluid flux through sediment on the western flank of the Mid-Atlantic Ridge: A hydrogeological study of North Pond, *Geophys. Res. Lett.*, *19*, 517–520, 1992.

Larson, R. L., A. T. Fisher, and R. Jarrard, Highly layered and permeable Jurassic oceanic crust in the western Pacific, *Earth. Planet. Sci. Lett.*, *119*, 71–83, 1993.

Matthews, M., M. Salisbury, and R. Hyndman, Basement logging on the Mid-Atlantic Ridge, Deep Sea Drilling Project Hole 395A, in *Initial Reports, Deep Sea Drilling Project*, edited by R. D. Hyndman and M. H. Salisbury, vol. 78, pp. 717–730, U.S. Govt. Print. Off., Washington, D. C., 1984.

Mottl, M. J., and C. G. Wheat, Hydrothermal circulation through mid-ocean ridge flanks: Fluxes of heat and magnesium, *Geochim. Cosmochim. Acta*, *58*, 2225–2237, 1994.

Mottl, M. J., et al., Warm springs discovered on 3.5 Ma oceanic crust, eastern flank of the Juan de Fuca Ridge, *Geology*, *26*, 51–54, 1998.

Nield, D. A., Onset of thermohaline convection in a porous medium, *Water Resour. Res.*, *4*, 553–560, 1968.

Nield, D. A., and A. Bejan, *Convection in Porous Media*, 546 pp., Springer-Verlag, New York, 1999.

Parsons, B., and J. G. Sclater, An analysis of the variation of ocean floor bathymetry and heat flow with age, *J. Geophys. Res.*, *82*, 803–829, 1977.

Rosenberg, N., A. Fisher, and J. Stein, Large-scale lateral heat and fluid transport in the seafloor: Revisiting the well-mixed aquifer model, *Earth. Planet. Sci. Lett.*, *182*, 93–101, 2000.

Sanford, W. E., Correcting for diffusion in Carbon-14 dating of ground water, *Ground Water*, *35*(2), 357–361, 1997.

Shapiro, A. M., Effective matrix diffusion in kilometer-scale transport in fractured rock, *Water Resour. Res.*, *37*(3), 507–522, 2001.

Shapiro, A. M., and P. A. Hsieh, How good are estimates of transmissivity from slug tests in fractured rocks?, *Ground Water*, *36*(1), 37–48, 1998.

Stein, C., and S. Stein, Constraints on hydrothermal heat flux through the oceanic lithosphere from global heat flow, *J. Geophys. Res.*, *99*, 3081–3095, 1994.

Sudicky, E. A., and E. O. Frind, Carbon 14 dating of groundwater in confined aquifers: Implications of aquitard diffusion, *Water Resour. Res.*, *17*(4), 1060–1064, 1981.

Thomson, R. E., E. E. Davis, and B. J. Burd, Hydrothermal venting and geothermal heating in Cascadia Basin, *J. Geophys. Res.*, *100*, 6121–6141, 1995.

Tsang, C. F., and I. Neretnieks, Flow channeling in heterogeneous fractured rocks, *Rev. Geophys.*, *36*(2), 275–298, 1998.

Wang, K., J. He, and E. E. Davis, Influence of basement topography on hydrothermal circulation in sediment-buried oceanic crust, *Earth. Planet. Sci. Lett.*, *146*, 151–164, 1997.

Wheat, C. G., H. Elderfield, M. J. Mottl, and C. Monnin, Chemical composition of basement fluids within an oceanic ridge flank: Implications for along-strike and across-strike hydrothermal circulation, *J. Geophys. Res., 105*(B6), 13,437–13,447, 2000.

Yang, J., R. N. Edwards, J. W. Molson, and E. A. Sudicky, Fracture-induced hydrothermal convection in the oceanic crust and the interpretation of heat-flow data, *Geophys. Res. Lett.*, *23*, 929–932, 1996.

Zyvoloski, G. A., B. A. Robinson, Z. D. Dash, and L. L. Trease, Users manual for the FEHMN application, Los Alamos Natl. Lab., Los Alamos, N. M., 1996.